International Journal of Systems , Algorithms & Applications

Reynolds-Averaged Navier-Stokes Computations over a Two-element Aerofoil

[1]*Sharanappa V. Sajjan*, [2]*K. Siva Kumar*
[1,2]*Computational and Theoretical Fluid Dynamics Division, Council of Scientific and Industrial Research-National Aerospace Laboratories, Bangalore, Karnataka-560017, India*
e-mail: *svsajjan@ctfd.cmmacs.ernet.in*[1], *shivak@ctfd.cmmacs.ernet.in*[2]

Abstract **- Steady two-dimensional Reynolds-averaged Navier-Stokes computations are performed for the flow around a NLR7301 aerofoil-flap configuration with flap deflected over 20° at different angles of attack. The Implicit Reynolds-averaged Navier-Stokes solver (IMPRANS) used for obtaining solutions is based on finite volume nodal point spatial discretization scheme. Baldwin and Lomax turbulence model has been used for the turbulence closure. The main aim is to show the applicability of the existing solver for multi-element aerofoil applications. The results are presented in the form of surface pressure and aerodynamic coefficients and compared with available experimental results.**

Keywords: *RANS solver; implicit method; dual time stepping; two-element aerofoil*

I. INTRODUCTION

The problem of maximum lift prediction is challenging for both experiments and CFD due to the mix of complex flow phenomena involved such as transition, separation, low subsonic flow combined with transonic flow (on the slat), wake-boundary layer confluence, etc. The analysis and design of multi-element high lift systems for aircraft also has become increasingly important. Where early attention was mostly focused on maximum lift requirements to satisfy the high cruise wing loading for transport aircraft while retaining acceptable take-off and landing distances, more recently the attention has turned to reducing the complexity of the high-lift systems for given maximum lift levels. Also, the high lift systems are desired to maintain low drag at take-off so as to attain cruise speed faster and high drag at approach. Therefore there is a need to have simpler high lift systems which are cheaper in terms of manufacturing and maintenance cost. Multi-element aerofoils are in common use on fixed wing aircraft. In such conventional applications, the aerodynamic flow environment is steady or quasi-steady. These aerofoil sections are designed specifically for high angles of attack and low Mach number conditions.

Cebeci [1] has done experiments on multi-element aerofoils which show that the compressibility effect, even at Mach numbers around 0.3, has a pronounced effect on the maximum lift coefficient. Similarly the predicted location of transition in the calculation method is important in properly identifying the effects of wind tunnel and flight Reynolds numbers. Individual components of multi-element aerofoils at wind tunnel Reynolds numbers can experience relatively lower Reynolds numbers than the main aerofoil. At chord Reynolds numbers less than 500,000; the components can have large separation bubbles, with the onset of transition occurring inside the separation bubble.
Van den Berg and Gooden [2] are conducted an experiment and the test data are given for a two-dimensional wing flap configuration NLR 7301 with flap, which has been so designed that nowhere flow separations occur, apart from a small laminar separation bubble on the wing nose. The 32% chord trailing edge flap is deflected 20°. Two widths of the gap between wing and flap have been applied, with mixing of the wing wake and flap boundary layer occurring with the smaller gap. The experiment has been carried out at a Reynolds number of 2.51×10^6 and a Mach number of about 0.185. The measurements comprise surface pressure data, from which lift and pitching moment coefficients were calculated, at various angles of attack from zero up to beyond stall. At three angles of attack the drag has been determined from wake traverses. At these angles mean flow measurements in the boundary layer and wake have been executed at 16 stations. In addition turbulence data were obtained at 5 stations in the wing wake above the flap.
Smith [3] has described about the high-lift aero-dynamics, in that he has developed some powerful methods of calculating potential and boundary layer flows on multi-element aerofoils.
In *Cebeci et al. [4]*, a calculation method for multi-element aerofoils based on an interactive boundary-layer approach using an improved Cebeci-Smith eddy viscosity formulation is described.
Kyle Anderson [5] performed Navier-Stokes computations on multi-element aerofoils. They obtained results for both landing and take-off multi-element aerofoils for a variety of Mach number and Reynolds number combinations up to the flight conditions. Effects on maximum lift are considered for the landing configurations and effects on both lift and drag are reported for take-off geometry.

In this paper, the results are obtained using Implicit Reynolds-averaged Navier-Stokes (IMPRANS) solver are presented in the form of aerodynamic coefficients such as lift, drag, moment and surface pressure coefficient. The NLR7301 aerofoil-flap configuration is used with the flap deflected over 20.0° which is shown in Fig. 1. The configuration is designed in such a way that the flow is attached to the aerofoil surface for more than 10° angle of attack. Present simulations are performed at angles of attack of 0.0°, 6.0°, 10.1°, 13.1° and 20.0° they are compared with the available experimental results of [2].

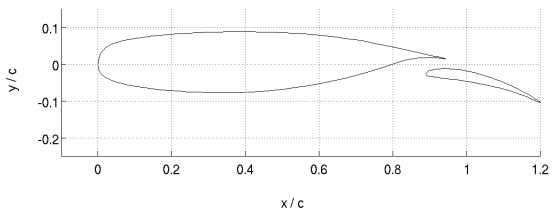

Figure 1: The NLR7301 aerofoil with the flap deflected over 20.0°

International Journal of Systems , Algorithms & Applications

II. IMPRANS SOLVER

The two-dimensional Reynolds-averaged Navier-Stokes equations for a moving domain can be written in non-dimensional conservative form a

$$\frac{\partial U}{\partial t}+\frac{\partial F}{\partial x}+\frac{\partial G}{\partial y}=\frac{\partial V}{\partial x}+\frac{\partial W}{\partial y} \qquad (1)$$

where

$$U=\begin{bmatrix}\rho\\ \rho u\\ \rho v\\ e\end{bmatrix},\quad F=\begin{bmatrix}\rho(u-x_t)\\ \rho u(u-x_t)+p\\ \rho v(u-x_t)\\ e(u-x_t)+pu\end{bmatrix},\quad G=\begin{bmatrix}\rho(v-y_t)\\ \rho u(v-y_t)\\ \rho v(v-y_t)+p\\ e(v-y_t)+pv\end{bmatrix} \qquad (2)$$

$$V=V_1(U,U_x)+V_2(U,U_y)$$

$$=\frac{1}{Re_\infty}\begin{bmatrix}0\\ \lambda(u_x+v_y)+2\mu u_x\\ \mu(v_x+u_y)\\ \mu v(u_y+v_x)+\lambda u(u_x+v_y)+2\mu u u_x+\dfrac{\mu T_x}{(\gamma-1)M^2_\infty Pr}\end{bmatrix} \qquad (3)$$

$$W=W_1(U,U_x)+W_2(U,U_y)$$

$$=\frac{1}{Re_\infty}\begin{bmatrix}0\\ \mu(u_y+v_x)\\ \lambda(u_x+v_y)+2\mu v_y\\ \mu u(u_y+v_x)+\lambda v(u_x+v_y)+2\mu v v_y+\dfrac{\mu T_y}{(\gamma-1)M^2_\infty Pr}\end{bmatrix} \qquad (4)$$

Here x and y are the Cartesian coordinates and t is the time variable; x_t and y_t are the Cartesian velocity components of the moving domain. For a fixed domain, the grid speeds x_t and y_t are zero. U is the vector of conserved variables; F, G are inviscid flux vectors and V, W are viscous flux vectors.

The primitive variables are density ρ, velocity components u, v in the x and y directions, pressure p, temperature T and total energy e per unit volume. The non-dimensional variables used in the above equations have been obtained by using the following free stream values as reference quantities:
ρ_∞ (density), U_∞(velocity), μ_∞ (viscosity), $\rho_\infty U^2_\infty$ (pressure), T_∞(temperature), and so on. Some characteristic length such as chord c of an aerofoil is chosen as the length scale.

M_∞ and Re_∞ are the free stream Mach number and Reynolds number respectively; γ is the ratio of specific heats and Pr is the Prandtl number. In addition, the viscosity coefficients λ and μ given by the Stokes relation

$$3\lambda + 2\mu = 0 \qquad (5)$$

and the Sutherland's law of viscosity

$$\mu = C_1\left[\frac{T^{3/2}}{T+C_2}\right] \qquad (6)$$

For turbulent flows, the laminar viscosity coefficient μ is replaced by $\mu + \mu_t$, and μ / Pr is replaced by $\mu / Pr + \mu_t / Pr_t$; the turbulent viscosity coefficient μ_t and the turbulent Prandtl number Pr_t are provided by a turbulence model. Finally the system is closed using the perfect gas equation of state in non-dimensional form as

$$P=\frac{\rho T}{\gamma M^2_\infty} \qquad (7)$$

The Euler equations for inviscid flow are obtained from the Navier-Stokes equations by setting

$$\frac{1}{Re_\infty}=0$$

III. COMPUTATIONAL METHOD

Applying Euler's implicit time differencing formula [6]

$$U^n = U^{n+1} - \left(\frac{\partial U}{\partial t}\right)^{n+1}\Delta t + O\left(\Delta t^2\right) \qquad (8)$$

to the governing Eq. (1), we obtain

$$\Delta U^n + \Delta t\left[\frac{\partial}{\partial x}(F-V)+\frac{\partial}{\partial y}(G-W)\right]^{n+1}=0 \qquad (9)$$

Here $U^n = U(t) = U(n\,\Delta t)$ is the solution vector at time level n and $\Delta U^n = (U^{n+1} - U^n)$ is the change in U^n over time step Δt. In order to facilitate the finite volume formulation, the above equations are written in the integral form as

$$\iint_\Omega \Delta U^n dx dy + \Delta t\int_\Gamma\left[(F-V)^{n+1}dy-(G-W)^{n+1}dx\right]=0 \qquad (10)$$

where Ω is any two-dimensional flow domain and Γ is the boundary curve.

In the nodal point finite volume approach [7, 8], the flow variables are associated with each mesh point of the grid and the integral conservative equations are applied to each control volume obtained by joining the centroids of the four neighbouring cells of a nodal point. Application of nodal point spatial discretization to Eq. (10) leads to the following equations for the computational cell Ω_{ij}

$$\Delta U^n_{ij} h_{ij} + \Delta t\int_{\Gamma_{ij}}\left[(F-V)^{n+1}dy-(G-W)^{n+1}dx\right]=0 \qquad (11)$$

Linearizing the changes in flux vectors using Taylor's series expansions in time and assuming locally constant transport properties, Eq. (11) can be simplified to

$$\Delta U^n_{ij}+\frac{\Delta t}{h_{ij}}\left[\int_{\Gamma_{ij}}\left\{A^n-\frac{\partial}{\partial x}R^n\right\}\Delta U^n dy-\int_{\Gamma_{ij}}\left\{B^n-\frac{\partial}{\partial y}S^n\right\}\Delta U^n dx\right]$$
$$=-\frac{\Delta t}{h_{ij}}\left[\int_{\Gamma_{ij}}(F-V)^n dy+\int_{\Gamma_{ij}}(G-W)^n dx\right] \qquad (12)$$

Here A, B, R and S are the Jacobian matrices which are given by

$$A=\frac{\partial F}{\partial U},\ B=\frac{\partial G}{\partial U},\ R=\frac{\partial V_1}{\partial U_x}\ \text{and}\ S=\frac{\partial W_2}{\partial U_y} \qquad (13)$$

International Journal of Systems , Algorithms & Applications

This RANS solver has been extensively validated for computing unsteady flow past pitching aerofoils and wings [9], plunging aerofoils and wings [10], flapping aerofoils [11], helicopter rotor blades [12, 13], wind turbines [14] etc. Here, the solver has been applied for computing two-dimensional steady flow over a two-element NLR7301 aerofoil with flap configuration.

IV. GRID GENERATION

For all present computations, the structured, two-block, C-type grid of block sizes 405×65 and 72×35 (stream-wise × normal) over NLR7301 aerofoil with flap is used which is shown in Fig. 2(a). The outer block starts from the far field boundary in the wake to far field boundary in the upstream of leading edge and back to the wake boundary. The second block of grid is generated in gap between main aerofoil and the flap. 289 points are distributed on the main aerofoil surface, 219 points on the flap and 41 points in the wake region. The outer boundary is located 30 chords away from the aerofoil surface. The first grid spacing on the aerofoil surface of 1.0×10^{-5}c was used in the direction normal to the aerofoil surface. The grid points are properly clustered near the leading, trailing edges, in the gap between aerofoil-flap and wall normal direction. The close-up view of the grid is shown in Fig. 2(b).

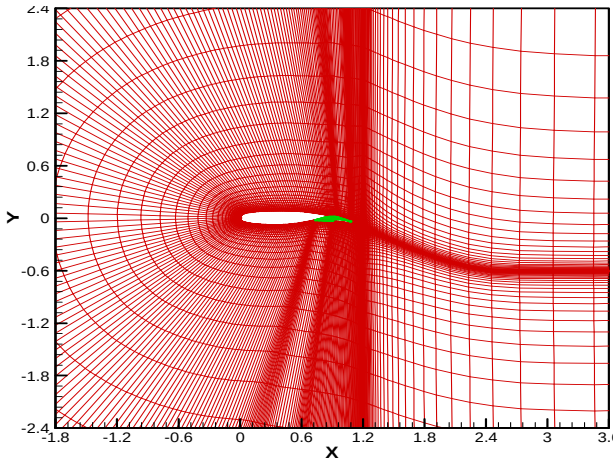

Figure 2(a): C-grid around the NLR 7301 aerofoil-flap configuration

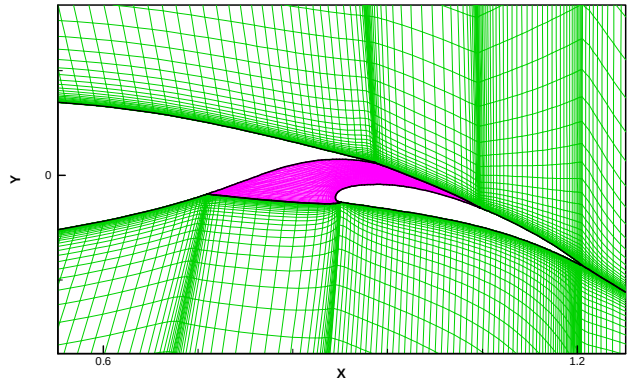

Figure 2(b): Close-up view of the grid around aerofoil-flap configuration

V. RESULTS

The Reynolds averaged Navier-Stokes simulations are presented for the steady flow over a NLR7301 aerofoil-flap configuration with the flap deflected over 20° degrees. The results are obtained using implicit RANS solver IMPRANS with Baldwin and Lomax turbulence model at angles of attack of 0.0°, 6.0°, 10.1°, 13.1° and 20.0°. The predicted values are compared with the available experimental results of [2] at Mach number = 0.185 and Reynolds number = 4.0 million.

The coefficient of surface pressure versus *x*/*c* over the main element and the flap at different angles of attack has been shown in Fig. 3 along with the available experimental data. The comparison is good in all the cases considered. The surface pressure field plots along with the stream lines are shown in Fig. 4 for different angles of attack. From the figure it is seen that the higher pressure on the lower surface of both aerofoil and flap and lower pressure on the upper surfaces. As the angle of attack to the aerofoil-flap configuration increases the pressure on lower surface increases. In these simulations up to 10.1° angle of attack the flow is attached to the main aerofoil and the flap.

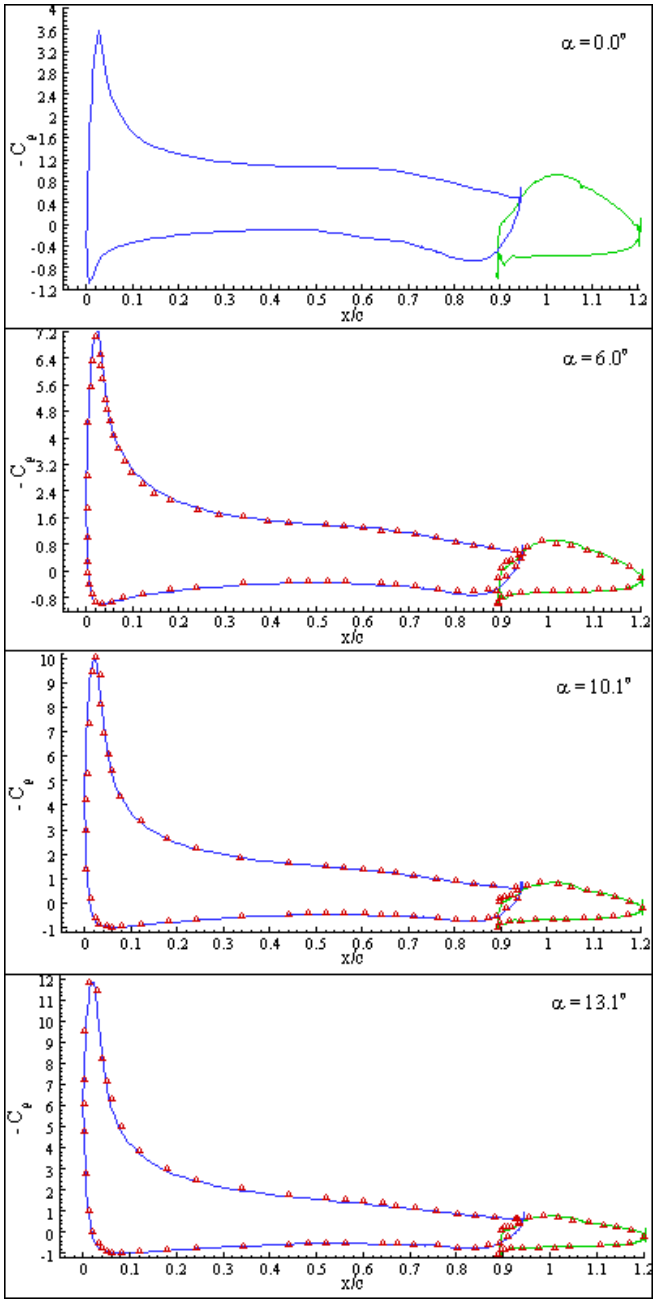

Figure 3: Surface pressure distribution at different angles of attack on aerofoil-flap configuration at M_∞ = 0.185, *Re* = 4.0 million
Main element (Present), Flap (Present), Δ Experiment

IJSAA International Journal of Systems , Algorithms & Applications

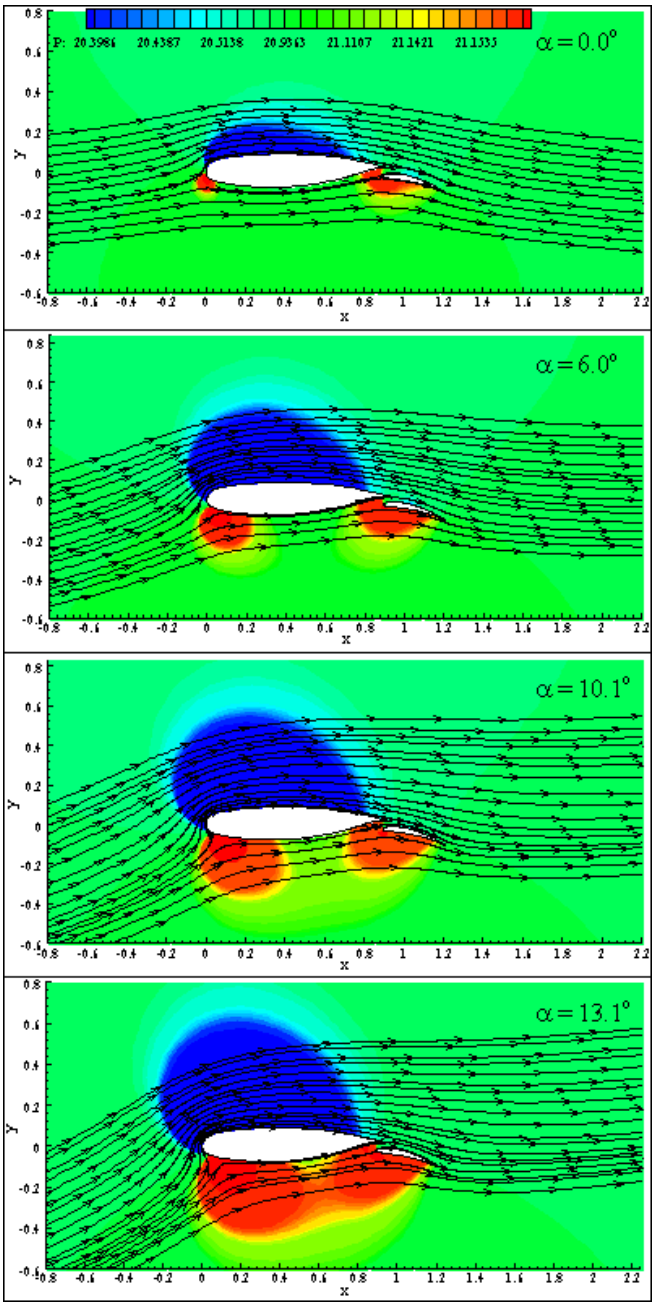

Figure 4: Pressure and streamline contour at different angles of attack on aerofoil-flap configuration at M_∞ = 0.185, *Re* = 4.0 million

Only at angle of attack of 13.1° the flow reversal is seen from the trailing edge separation. Further increase in angle of attack to 20°, the flow separates from the leading edge and forms a large leading edge vertex and sheds in the wake as shown in Fig. 5.

The aerodynamic coefficient values over the aerofoil-flap configuration at different angles of attack are listed in Table 1 for both experimental and the present calculations.

It should be mentioned here that the values in Table 1 are the coefficients for the complete configuration. They consist of the forces on both main element and the flap.

The aerodynamic moment is calculated with respect to the quarter-chord point (x/c = 0.25). Further from Table 1 it can be seen that the difference between the simulation results and the measurements. The difference is increased as angles of attack increases; the present predicted values are lower but still reasonable. Obviously, cases with higher angles of attack becomes more difficult, compared to the cases with lower angles of attack, because of flow separation and larger pressure gradients. This difference could also be due to the Baldwin and Lomax turbulence model used in the present calculations.

Table 1: Comparison of Aerodynamic Coefficients

α	Experimental values			Present computed results		
	C_l	C_d	C_m	C_l	C_d	C_m
0.0°	1.64	-	0.457	1.51	0.058	0.365
6.0°	2.41	0.040	0.471	2.31	0.051	0.384
10.1°	2.87	0.056	0.463	2.67	0.045	0.355
13.1°	3.14	0.044	-	2.89	0.061	0.338

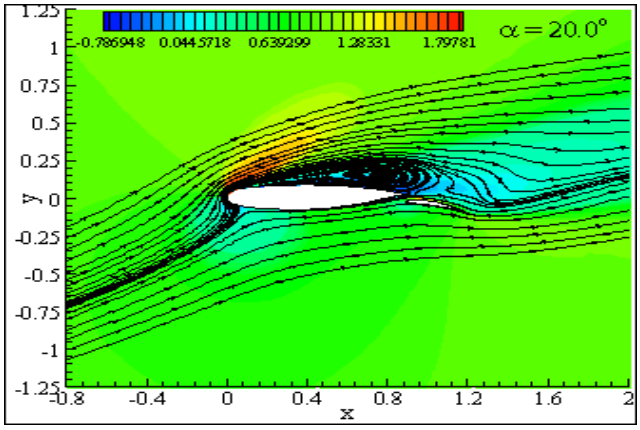

Figure 5: Pressure and streamline contour on aerofoil-flap configuration at an angles of attack of 20° and M_∞ = 0.185, *Re* = 4.0 million

VI. CONCLUDING REMARKS

The steady flow over a two-element aerofoil-flap configuration has been simulated using IMPRANS solver at different angles of attack. The RANS solver has been modified to handle multiple bodies. The results are compared with the available experimental values at different angles of attack. A case at high angle of attack has been computed to show the flow separation over the main aerofoil.

ACKNOWLEDGMENT

The authors gratefully acknowledge Dr. P. K. Dutta for his constant encouragement and support during the work.

REFERENCES

[1] T. Cebeci, “Essential Ingredients of a Method for Low Reynolds-Number Aerofoils”, AIAA Journal, Vol. 27, 1983, pp. 1680-1688.

[2] Van den Berg and Gooden, AGARD, “A selection of experimental test cases for the validation of cfd codes”, Advisory Report 303, A9-1, Vol. No. 2, August 1994.

[3] A. M. O. Smith, “High-Lift Aerodynamics” Journal of Aircraft, Vol. 12, No. 6, June 1975.

[4] T. Cebeci, Eric Besnard and Hsun H. Chen “Calculation of Multi -element Airfoil flows, including Flap wells” AIAA 96-0056, 1996.

[5] W. Kyle Anderson, Daryl L. Bonhaus, Robert J. McGhee and Betty S. Walker, “Navier-Stokes Computations and Experimental Comparisons for Multi-element Airfoil Configurations”, Journal of Aircraft, Vol. 32, No. 6, November-December 1995.

[6] R. M. Beam and R. F. Warming, 1978. An Implicit Factored Scheme for the Compressible Navier-Stokes Equations, AIAA Journal, Vol. 16, No. 4, pp. 393 - 402.

[7] M. G. Hall, 1985. Cell Vertex Multi-grid Scheme for Solution of the Euler Equations RAE-TM-Aero 2029, Proc. Conf. on Numerical methods for fluid dynamics, pp. 303 - 345.

[8] A. Jameson, W. Schmidt and E. Turkel, 1981. Numerical Solution of Euler Equations by Finite Volume Methods Using Runge Kutta Time Stepping Schemes, AIAA Paper 81 – 1259.

[9] Sharanappa V. Sajjan, Vimala Dutta and P. K. Dutta 2008. Numerical Simulation of flow over pitching bodies using an implicit Reynolds-averaged Navier-Stokes solver, Proc. of 12th Asian congress of Fluid Mechanics, Daejeon, Korea.

[10] K. Siva Kumar and Sharanappa V. Sajjan, "Unsteady Compressible Flow over Heaving Bodies using an Implicit RANS Solver", International Journal on "Applied Mechanics and Materials", Vols. 110 - 116 (2012), pp 4589 - 4597.

[11] Sharanappa V. Sajjan and K. Siva Kumar, "Parametric Study of Flapping Motion of an aerofoil", Proceedings of International Conference on Computing, Communications, Systems and Aeronautics (ICCCSA-12), Hyderabad, 30th - 31st, March 2012.

[12] Vimala Dutta, Sharanappa and P. K. Dutta, 2005. Navier-Stokes Computations for a Helicopter Rotor Blade in Hover, Proc. Eighth Annual CFD Symposium, CFD Division of Aeronautical Society of India, Bangalore, CP 18.

[13] Sharanappa V. Sajjan, Vimala Dutta, and P. K. Dutta, 2006. Viscous Unsteady Flow around a Helicopter Rotor Blade in Forward Flight. Proc. 9th Annual CFD symposium, CFD Division of Aeronautical Society of India, Bangalore.

[14] P. K. Dutta, Vimala Dutta, and Sharanappa V. Sajjan., 2007. RANS Computation of Flow past Wind Turbine Blades. Proc. of 7th Asian Computational Fluid Dynamics Conference, Bangalore (Invited Paper).